Emission-line polarization degrees and $n\ell m_\ell$ distributions produced by state-selective electron capture in slow Kr^{8+}-Li($2s$) collisions

E. Jacquet,[1,2] H. Kucal,[1,2] V. Bazin,[1] P. Boduch,[1,2] M. Chantepie,[1,2] G. Cremer,[1,2] C. Laulhé,[1] and D. Lecler [1]
[1]*Centre Interdisciplinaire de Recherche Ions Lasers, UMR 6637 CEA-CNRS-ISMRA, Université de Caen, ISMRA, 6 Boulevard Maréchal Juin, F-14050 Caen Cedex 4, France*
[2]*UFR des Sciences, Université de Caen Basse Normandie, Boîte Postale 5186, F-14032 Caen Cedex, France*

J. Pascale
Service des Photons, Atomes et Molécules, CEA, Centre d'Etudes de Saclay, Bâtiment 522, F-91191 Gif-sur-Yvette Cedex, France
(Received 15 February 2000; revised manuscript received 14 April 2000; published 19 July 2000)

Polarization degrees of lines emitted by Kr^{7+} excited ions produced by single-electron capture during $Kr^{8+}+Li(2s)$ collisions were experimentally measured for projectile energies between 0.1 and 2.5 keV amu^{-1}. They were compared with theoretical polarization degrees obtained from $n\ell m_\ell$ distributions calculated by using the classical trajectory Monte Carlo (CTMC) method; radiative cascades have been included in the calculations. The fair agreement between experimental and calculated polarization degrees confirms the reliability of the CTMC method and allows one to analyze the m_ℓ distributions in terms of dynamical couplings responsible for the state-selective electron capture process.

PACS number(s): 34.10.+x, 34.70.+e

I. INTRODUCTION

Collisions between very slow Kr^{8+} ions and lithium atoms in their ground state are performed for collision energies between 0.1 and 2.5 keV amu^{-1} by high-resolution photon spectroscopy in the 200–600 nm wavelength range. For this collision energy range, the prevailing process is the capture of the $2s$ electron of the lithium atom into 7ℓ, 8ℓ, and 9ℓ sublevels of the Kr^{7+} alkali-metal ion [1]. Our interest is focused here on the m_ℓ distributions of the most populated $n\ell$ sublevels. These m_ℓ distributions indicate the degree of alignment of the produced states and consequently reflect, through this geometrical effect, the mechanisms involved during the collision [2].

This study follows several other studies dealing with collisions between stripped or fully stripped ions and alkali-metal targets.

Gauntt and Danzmann [3] have measured the intensities and polarization degrees of fine-structure lines in the $N=9-8$ manifolds of Ne VIII and Ar VIII spectra produced in collisions of very slow ($v=0.05$–0.15 a.u. Ne^{8+} and Ar^{8+} ions with atomic sodium. They have determined alignment and partial cross sections for electron capture as functions of projectile energy. For the neon projectiles, the polarization of the Bohr line is approximately 0.3 and independent of velocity; for argon projectiles, the polarization is about 0.15 and increases with increasing velocity.

Schippers *et al.* [4] have investigated m_ℓ distributions of the He II ($n=4$) states formed during $He^{2+}+Na(3s)$ collisions by measuring the linear polarization of the He II ($4\rightarrow3$) emission. Over the energy range investigated (2–13.3 keV amu^{-1}), the polarization of the line they have measured increases from 0.2 to 0.3 indicating a strong alignment of the captured projectile charge cloud along the internuclear axis. The same group [5] have also studied the C^{3+} ($6\rightarrow5$) emission line at 465.7 nm emitted in C^{4+}-Na($3s$) collisions over the 3–7 keV amu^{-1} energy range. The polarization is found to be 0.33 and independent of the collision energy. In both cases, classical trajectory Monte Carlo (CTMC) calculations agree with the experimental findings indicating preferential capture into $m_\ell=0$ states.

We have previously studied both experimentally and theoretically the influence of the projectile energy on the m_ℓ distributions of the Ar^{7+} excited states produced by electron capture during Ar^{8+}-Li($2s$) collisions in the 0.1–4.5 keV amu^{-1} energy range [6,7]. By measuring the polarization of the emitted light, we have investigated, for the levels $n=8$ and 9 which are the most populated by the single electron-capture process, the $7\ell'$-8ℓ and $8\ell'$-9ℓ radiative transitions subsequent to the decay of the 8ℓ and 9ℓ sublevels of Ar VIII. The experimental polarization degrees were found in agreement with those obtained from CTMC calculated m_ℓ-distributions and dynamical couplings between the relevant electronic potential-energy curves for the $\{Ar^{7+}+Li\}^{+}$ molecular system. In particular, a projectile core-electron effect was demonstrated at low energies from additional CTMC calculations for the O^{8+} projectile. For the highest energy investigated (4.5 keV amu^{-1}), the polarization ratios corresponding to transitions involving high angular momentum value states reach 30%. For the 1.5–4.5 keV amu^{-1} energy range, the polarization ratios decrease slightly when the energy decreases; for projectile energies lower than 1.5 keV amu^{-1}, the polarization ratios decrease strongly with the energy. In the case of $7\ell'$-8ℓ transitions, this strong decrease is followed by an increase at the lowest energies. The large polarization ratios indicate that, after the collision, the electronic cloud tends to be aligned parallel to the incident ion beam direction. It means that the probability of capture into sublevels with low m_ℓ values ($m_\ell=0,\pm1,\pm2$) is enhanced for the highest energies investigated, show-

ing that the Stark effect and intershell rotational couplings are effective. According to a discussion based on electronic energy curve calculations, we have shown that the strong decrease of polarization degrees with decreasing energies in the case of the Ar^{8+}-Li($2s$) collisional system is due to a decrease of the intershell rotational couplings while the intrashell rotational couplings remain effective to populate large value of m_ℓ. At very low energies and for high angular momentum value states, the radial couplings become efficient while the rotational couplings are weakened; this results in an increase of the polarization for the emission lines of the capture levels.

In order to investigate experimentally the influence of the projectile core electrons on the final $n\ell$ distributions of the electron capture, the Kr^{8+}-Li($2s$) collision has been recently studied [1]. As for the Ar^{8+}-Li($2s$) collision, the most populated levels are $n=8$ and $n=9$ states, but, because of the overlapping of the various manifolds, the $7d$, $7f$, $7i$, $10s$, and $10p$ states are also populated especially for the lowest energies. The 8ℓ- and 9ℓ-distributions have been experimentally determined for collision energies between 0.1 and 1.5 keV amu^{-1} and theoretically calculated by using the CTMC method between 0.1 and 5.0 keV amu^{-1}. In spite of some discrepancies, experimental and theoretical results are in fair agreement. The analysis of the molecular electronic energy curves of the $\{Kr^{7+}+Li\}^{+}$ molecular (which presents particular features with respect to the $\{Ar^{7+}+Li\}^{+}$ system due to the overlapping of the various manifolds of molecular energy curves) in connection with the CTMC results of the $\sigma(n\ell)$ cross sections has shown the first importance of primary radial couplings for populating the nondegenerate $n\ell$ levels (low ℓ values) and the importance of the Stark effect due to the residual Li^{+} ion for populating degenerate $n\ell$ levels (high ℓ values) from nf and ng states and probably also from $(n+1)p$ levels by rotational coupling. In the present paper, we extend the experimental study of the projectile core electron influence on the $n\ell$ distributions to that on the m_ℓ distributions. Using the same experimental setup as for the Ar^{8+}-Li($2s$) collision [6,7], the polarization degrees have been measured for the Kr^{8+}-Li($2s$) collision in the 0.1–2.5 keV amu^{-1} energy range, for transitions from the most populated levels. The experimental techniques will be recalled. The polarization degrees are then compared with those obtained from the CTMC calculated m_ℓ distributions, by a method which is described in more details than in our similar study for the Ar^{8+} projectile, while the well-known CTMC method is just outlined. The CTMC calculations have been extended to energies up to 5 keV amu^{-1}. As for the Ar^{8+}-Li($2s$) collisional system, the experimental polarization degrees are then analyzed from the CTMC results. The calculated polarization degrees are discussed in terms of final m_ℓ distributions and then in terms of dynamical couplings responsible for the state-selective electron-capture processes, from an analysis of electronic energy curves of the $\{Kr^{7+}+Li\}^{+}$ system. Finally, they are compared with the CTMC results obtained for the Ar^{8+}-Li($2s$) and O^{8+}-Li($2s$) collisional systems.

II. EXPERIMENT

A. Experimental measurements of polarization rates

The krypton ions were produced by an ECR source of the GANIL[1] test bench; they were extracted from the ion source with a potential $U_0=12$ kV, corresponding to the maximum efficiency of the source. After a charge and mass analysis, the Kr^{8+} ion beam was focused inside a collision chamber on an effusive jet of lithium atoms provided by an oven. Since the energy range (0.1–2.5 keV amu^{-1}) investigated here cannot be provided directly with the ion source, the ion energy was modified just before the collision area. For collision energies lower than 1.0 keV amu^{-1}, the ions were decelerated before the lithium jet and reaccelerated after in order to be analyzed by a Faraday cup. For collision energies larger than 1.5 keV amu^{-1}, the ions were accelerated before the collision area and decelerated after. The decelerating device has already been described several times [6,8,1] together with the optical device used for polarization measurements.

Photons emitted in Kr^{8+}-Li($2s$) collisions were detected in the direction perpendicular to the ion beam and the lithium jet. They were wavelength-selected by a grating spectrometer in the 200–600 nm range. The polarization of each line was measured using a polarimeter composed of two polarizers: the polarization direction of the first one can be oriented parallel or perpendicular to the direction of the ion beam; the second one is a Glan-Taylor prism and its polarization direction is fixed at 45° to the ion beam direction. It compensates for the polarization effects of the spectrometer (grating and mirror). The polarization degree is defined by

$$P=\frac{I_{\parallel}-I_{\perp}}{I_{\parallel}+I_{\perp}}, \tag{1}$$

where $I_{\parallel}$ and $I_{\perp}$ are the intensities of the emitted light polarized along or perpendicular to the ion beam direction.

B. Experimental results

As we have shown, during Kr^{8+}-Li($2s$) collisions, the single electron-capture process populates the Kr^{7+} excited configurations with $n=7$, 8, and 9. These states decay radiatively and we have observed the lines corresponding to transitions from these states [1]. For all these transitions, the polarization rates were measured for collision energies from 0.1 to 2.5 keV amu^{-1}.

The experimental polarization rates and their uncertainties versus the collision energy are reported in Table I. The accuracy of the determination of the polarization rate depends on the quality of the optical device but also on the errors in the reading of the recorded signals. However, preliminary tests with depolarized light of a mercury lamp and tests of polarization in the various diffraction orders have shown that the uncertainties due to the defects of the optical device could be neglected in comparison with those deduced from the recordings. The emitted intensities $I_{\parallel}$ and $I_{\perp}$ are defined,

[1]Grand Accélérateur National d'Ions Lourds, Caen, France.

TABLE I. Experimental polarization rates (%) of the emission lines corresponding to $\Delta n=0$ and $\Delta n=1$ transitions resulting from single electron capture in Kr^{8+}-Li($2s$) versus collision energy (in keV amu^{-1}). No value is indicated when the line is too weak to measure the various intensities.

Transition \ Energy	0.1	0.2	0.5	0.8	1.0	1.4	1.5	2.0	2.5
$7p_{1/2}$-$7d_{3/2}$	7.0±3.7	−3.4±3.0	−4.9±1.4	−1.0±2.7	−2.8±3.0	−8.4±3.3			
$7p_{3/2}$-$7d_{5/2}$	7.2±3.2	−6.4±2.3	−4.6±2.8	−4.8±3.3	−2.9±3.4	−8.5±3.2			
$7d_{3/2}$-$7f_{5/2}$	9.7±4.1	3.2±3.6	0.0±2.7	−5.6±2.4	−6.1±5.4	−3.5±3.2	−5.1±2.6	−9.2±2.5	−5.6±2.6
$7d_{5/2}$-$7f_{7/2}$	11.6±2.9	1.5±1.8	0.3±4.9	−5.2±4.2	−6.0±4.0	−4.1±3.4	−4.6±3.7	−10.1±3.8	−4.0±4.0
$8p_{1/2}$-$8d_{3/2}$	13.1±8.4	−4.0±6.4	1.7±5.6	−3.1±4.6	−4.4±4.2				
$8p_{3/2}$-$8d_{5/2}$	6.5±9.7	0.4±6.1	3.6±4.8	1.5±4.0	5.2±3.5				
$8d_{5/2}$-$8f_{7/2}$	5.6±2.8	−15.1±2.6	−8.9±4.7	−8.5±5.2	−1.2±4.6		2.4±2.4	1.0±5.4	2.5±6.8
$6f_{5/2}$-$7d_{3/2}$	−0.3±3.2	0.0±0.1	0.4±1.5	0.3±0.4	−2.2±6.2	−3.1±3.5			
$6f_{7/2}$-$7d_{5/2}$	2.7±3.6	−2.3±6.2	−3.4±4.6	−1.0±4.2	−2.3±4.4	−3.5±4.1			
$6g$-$7h$					20.5±6.3				
$7d_{3/2}$-$8p_{1/2}$	2.5±6.6	−3.1±4.1	0.0±4.1	−2.6±3.8	1.2±5.4	−1.4±5.7			
$7d_{5/2}$-$8p_{3/2}$	0.8±5.2	−2.6±3.2	−2.3±3.9	−0.7±3.8	−2.6±4.2	−1.4±5.7			
$7f_{5/2}$-$8d_{3/2}$					−9.9±7.8				
$7f$-$8g$					21.9±8.1		6.1±8.2	18.8±6.4	12.5±6.1
$7g$-$8h$	15.1±2.8	7.4±3.7	13.0±4.0	13.0±4.0	11.7±3.6	15.2±3.3	17.6±2.9	20.4±2.2	21.8±5.1
$7h$-$8i$	7.0±3.5	8.0±2.3	18.3±2.7	23.6±3.6	21.6±2.8	21.5±1.7			
$7i$-$8k$	5.1±2.6	6.1±3.1	22.0±3.0	26.0±2.5	25.0±2.7	25.5±1.8	25.5±2.4	27.1±2.5	28.1±2.2
$8p_{1/2}$-$9s_{1/2}$					−2.5±5.4	−1.5±7.1			
$8p_{3/2}$-$9s_{1/2}$	−0.7±4.3	−2.4±2.8	−1.3±4.2	−0.9±2.8	−2.1±4.5	−1.9±5.6			
$8d_{3/2}$-$9p_{1/2}$	−3.5±3.5	0.8±2.2	−2.3±7.4	−0.5±6.2	−1.5±5.8				
$8d_{5/2}$-$9p_{3/2}$	8.3±3.9	−20.2±3.5	−22.2±4.4	−9.0±3.3	−11.4±6.8		4.7±6.4	15.9±6.4	3.0±9.5
$8f$-$9g$	24.6±5.7	22.7±6.3	21.4±3.3	18.1±3.3	20.3±8.1	22.0±7.2	18.3±6.0	16.6±4.8	19.2±4.7
$8g$-$9h$	19.8±4.3	22.5±4.3	23.8±2.7	24.4±2.4	22.2±4.0	23.7±4.0	24.9±3.7	24.9±3.0	28.3±2.7
$8h$-$9i$	19.2±4.0	24.4±3.2	27.4±2.9	26.7±2.4	22.3±2.4	25.8±1.7			
$8i$-$9k$/$8k$-$9l$					24.3±2.1	26.6±1.5	28.9±3.8	31.0±2.8	31.6±2.3

respectively, as $i_\parallel - i_{\min}$ and $i_\perp - i_{\min}$, where $i_\parallel$ and $i_\perp$ are the measured intensities recorded for the two polarization directions and $i_{\min}$, the intensity obtained for crossed polarizers. The experimental uncertainties were evaluated from the recordings and several measurements of each intensity were performed for each line in order to minimize the statistical errors.

The polarization rates of the lines emitted from states with large ℓ values are always positive. For the highest energies, the polarization rates reach values up to 30% and decrease with decreasing energies as already observed in the case of Ar^{8+}-Li($2s$) collisions. These states are always polarized along the ion beam direction.

The lines emitted from s and $p_{1/2}$ states are found to be unpolarized, showing that the optical device is well oriented. The lines emitted from states with low ℓ values (except s and $p_{1/2}$) and intermediate ℓ values are found to be weakly polarized or have negative polarization rates. Since these transitions involve rather small n values ($n=7$ and 8) and since the collision populates states up to $n=10$, one can expect that the cascade polarization effects are very important for these transitions.

III. CALCULATION OF POLARIZATION RATES

For a further analysis, the polarization rates have to be related to the population of m_ℓ magnetic sublevels. The polarization of a line can be expressed as a function of the m_ℓ distribution of the decaying level, taking the ion beam direction as the quantization axis. In the studied energy range, the collision time being small with respect to the spin-orbit interaction time, no change of spin occurs during the collision and only states with definite orbital angular momentum ℓ and its projection m_ℓ are populated.

However, the spin-orbit interaction has to be considered in the calculations of the intensity of the light emitted after the collision because spontaneous emission is much longer than spin-orbit interaction time.

An atomic excited state $|i\rangle$ will be described by its total angular momentum $\vec{J}_i$. It decays by spontaneous emission to another atomic state $|f\rangle$ with the angular momentum $\vec{J}_j$. The quantum numbers which correspond to the operators $\vec{J}_i$ ($\vec{J}_j$) and their projections along the quantization axis are denoted J_i (J_f) and m_i (m_f).

Following the theory developed by Fano and Macek [9],

the polarization rate of the emitted light corresponding to the transition between $|i\rangle$ and $|f\rangle$ can be expressed as a function of the alignment of the excited state $|i\rangle$ produced during the collision. Let us point out that, in our experimental setup characterized by a cylindrical symmetry, the alignment tensor has a single nonzero component: the longitudinal alignment A_0^2. In the basis $|J_i m_i\rangle$, A_0^2 is defined as follows:

$$A_0^2(J_i)=\frac{\sum_{m_i} 3m_i^2-J_i(J_i+1)\sigma(m_i)}{J_i(J_i+1)\sum_{m_i}\sigma(m_i)}, \tag{2}$$

where $\sigma(m_i)$ is the partial cross section for capture in the $|J_i m_i\rangle$ state.

Using the alignment parameter A_0^2, the expression of $P(i)$ takes a simple form:

$$P(i)=\frac{3h(i,f)A_0^2(J_i)}{4+h(i,f)A_0^2(J_i)}, \tag{3}$$

where

$$h(i,f)=(-1)^{J_i-J_f}\frac{\begin{Bmatrix} J_i & J_i & 2 \\ 1 & 1 & J_f \end{Bmatrix}}{\begin{Bmatrix} J_i & J_i & 2 \\ 1 & 1 & J_i \end{Bmatrix}} \tag{4}$$

and $\{{}^{J_i\ \ J_i\ \ 2}_{1\ \ 1\ \ J_f}\}$ is the 6-j symbol.

The simple algebraic theory allows us to express the $\sigma(m_i)$ cross section in terms of the $\sigma(\ell m_\ell)$ ones.

In our case, radiative cascades have to be taken into account. Radiative cascades from upper levels may produce a variation in the alignment of the studied levels since the alignment of the studied levels and the alignments of upper levels usually differ. The polarization rates are then directly affected by this transfer of alignment. The problem is to evaluate this transfer of alignment.

For the hydrogenlike ion, the problem of the transfer of alignment has been discussed in detail by Lin and Macek [10] and successfully applied to the states with unresolved fine structures. We have also observed transitions between fine-structure levels and we were able to experimentally determine the corresponding polarization rate (see Table I). In order to underline the radiative cascade effects and analyze our experimental data, we have directly applied the theory of Lin and Macek [10] to the $n\ell \rightarrow n'\ell'$ transitions and slightly modified their theory for the case of $n\ell J \rightarrow n'\ell' J'$ transitions. In the following, the main steps of this theory will be recalled.

Their calculation is based on anisotropy transfer theory. It means that, in the frame of the matrix density formalism, the kqth state multipole ${}^{J_i}\sigma_q^k$ is introduced for the given level J_i. This multipole allows us to calculate the values of anisotropy parameters, in particular the alignment parameter. If the two levels J_i and J_{i+1} are coupled by dipole radiative transitions and if LS coupling is valid, the relation between ${}^{J_i}\sigma_q^k$ and ${}^{J_{i+1}}\sigma_q^k$ can be easily deduced. It corresponds to the anisotropy transfer. Then, for each sequence of allowed transitions as $n_N\ell_N SJ_N \rightarrow n_{N-1}\ell_{N-1}SJ_{N-1}\rightarrow\cdots\rightarrow n_1\ell_1 SJ_1$, the relation between ${}^{J_i}\sigma_q^k$ and ${}^{J_N}\sigma_q^k$ is established, $n_N\ell_N SJ_N$ and $n_1\ell_1 SJ_1$ define the initial and final state linked by cascade. The ${}^{J_N}\sigma_q^k$ state multipole has to be expressed as a function of the ${}^{\ell_N}\sigma_q^k$ state multipole since the collision populates the ℓm_ℓ states.

Finally, assuming that the longitudinal alignment $A_0^2(\ell)$ is proportional to the expected value of the $3L_Z^2-L^2$ operator and that fine structure is not resolved for the final state, Lin and Macek [10] have carried out a linear relation between $A_0^2(\ell_1)$ and $A_0^2(\ell_N)$, namely $A_0^2(\ell_1)=\xi A_0^2(\ell_N)$. The definition of the parameter ξ can be found in Ref. [10].

In the same paper, the parameter ξ is numerically calculated for $S=\frac{1}{2}$ and $\ell=2$ to 9 for transitions with $\Delta\ell=1$. Actually, several cascade channels leading to the studied state i have to be taken into account; each cascade channel may contribute to the alignment transfer with various weights. Taking into account all the cascade channels, the alignment for the state i can be expressed as

$$A_0^2(\ell_i)=\frac{\sum_{j\geqslant i}\sum_k \omega_k(j)[\xi_k(j)A_0^2(\ell_j)]\sigma(j)}{\sum_{j\geqslant i}\sum_k \omega_k(j)\sigma(j)}. \tag{5}$$

In the expression (5), the sum is over all the cascade channels k and the initial states j, $\sigma(j)$ and $A_0^2(\ell_j)$ are, respectively, the production cross section and the initial alignment of state j, $\omega_k(j)$ is the branching ratio for the radiative transition from state j to state i via branch k, and $\xi_k(j)$ is the alignment transfer coefficient for the same radiative transition.

In the case of transitions between fine-structure levels, the polarization rate is given by expression (2), so we have to calculate $A_0^2(J)$. Using the Wigner-Eckart theorem, $A_0^2(J)$ is linked to $A_0^2(\ell)$ by the expression

$$A_0^2(J)=\frac{3X(X+1)-4J(J+1)\ell(\ell+1)}{2J(J+1)(2\ell+3)(2\ell-1)}A_0^2(\ell), \tag{6}$$

where $X=s(s+1)-J(J+1)-\ell(\ell+1)$ and $s=J+\ell+\frac{1}{2}$.

For transitions between fine-structure levels, the alignment $A_0^2(\ell)$ including radiative cascade effects is calculated using expression (5). $A_0^2(J)$ is deduced from $A_0^2(\ell)$ using expression (6).

IV. COMPARISON BETWEEN EXPERIMENTAL AND THEORETICAL POLARIZATION DEGREES

In order to analyze the experimental polarization rates, we have performed calculations of polarization rates using the method described above for the observed transitions. This method requires first to know the branching ratios and the $\sigma(n\ell m_\ell)$ cross sections.

For the branching ratios, we have used the same as those

TABLE II. CTMC m_ℓ distributions (%) versus the projectile energy (in keV amu^{-1}) for single electron capture into 7ℓ sublevels during Kr^{8+}-Li($2s$) collisions.

Sublevel \ Energy		0.1	0.2	0.5	0.8	1.0	1.4	2.0	3.0	4.0	5.0
$7s$	0	100.0	100.0	100.0	100.0	100.0	100.0	100.0	100.0	100.0	100.0
$7p$	0	100.0	25.0	37.8	29.5	25.6	22.1	33.6	26.4	29.3	31.4
	±1	0.0	37.5	31.1	35.2	37.2	38.9	33.2	36.8	35.3	34.3
7d	0	19.4	20.0	13.8	17.8	15.2	12.2	17.4	17.4	16.7	19.8
	±1	18.1	15.6	19.2	18.4	16.6	18.3	18.0	17.4	19.3	19.6
	±2	22.2	24.4	23.9	22.7	25.8	25.6	23.3	23.9	22.3	20.5
$7f$	0	15.0	16.3	9.8	11.8	9.5	12.5	10.8	9.7	11.9	13.7
	±1	15.6	17.1	13.0	9.7	11.1	9.2	11.7	10.6	11.3	12.2
	±2	14.2	13.4	12.4	12.4	12.6	11.1	10.8	13.2	14.0	14.0
	±3	12.8	11.3	19.7	22.0	21.5	23.4	22.1	21.3	18.7	17.0
$7g$	0	12.4	13.0	12.3	15.1	13.0	12.3	11.2	14.6	16.8	14.7
	±1	11.8	13.2	11.2	10.2	10.2	11.0	9.0	13.1	13.4	16.7
	±2	11.5	10.7	11.5	11.1	7.6	8.9	11.4	10.6	9.0	11.7
	±3	10.1	11.3	8.1	9.7	12.9	10.5	7.9	7.3	9.5	9.6
	±4	10.4	8.4	13.0	11.4	12.9	13.5	16.1	11.7	9.7	4.6
$7h$	0	6.2	10.1	10.0	7.0	11.1	10.5	15.0	17.5	19.2	14.0
	±1	7.0	6.4	7.6	8.4	8.6	10.9	12.7	13.8	12.3	13.0
	±2	9.0	8.1	8.1	7.6	9.0	8.9	9.2	10.0	10.5	10.9
	±3	8.1	8.9	8.8	9.4	7.4	7.4	6.0	6.2	9.0	10.4
	±4	12.6	10.1	9.3	9.4	9.5	6.3	4.6	7.2	6.5	7.0
	±5	10.1	11.5	11.2	11.7	9.9	11.3	10.0	4.0	2.1	1.7
$7i$	0	8.1	7.7	8.4	9.6	10.0	11.6	12.7	14.2	11.9	11.6
	±1	10.7	6.8	8.1	9.8	11.3	11.5	12.4	12.8	12.8	11.7
	±2	8.7	5.4	7.2	7.8	8.2	9.5	8.6	11.1	10.9	11.5
	±3	7.7	7.5	6.7	8.3	7.7	8.4	8.3	9.2	9.5	9.4
	±4	6.9	7.6	6.2	5.7	5.6	5.8	5.4	5.7	7.0	7.8
	±5	6.2	10.8	6.4	4.7	5.6	4.1	4.9	3.0	3.4	3.2
	±6	5.8	8.1	11.1	8.9	6.5	4.9	4.0	1.2	0.4	0.6

already calculated to determine the $\sigma(n\ell)$ cross sections for single electron capture into the $n=8$ and $n=9$ states of Kr^{7+} ions. Namely, the transition probabilities were calculated from radial matrix elements obtained with the parametric potential method of Klapish [11] optimized with some energy levels from Reader *et al.* [12,13].

The classical trajectory Monte Carlo (CTMC) method [14,15] has been used to calculate the $\sigma(n\ell m_\ell)$ cross sections. Indeed, we have already shown that the m_ℓ distributions calculated by the CTMC method can be used to calculate theoretical polarization rates [7]. These calculated polarization rates are in fair agreement with experimental results in the case of Ar^{8+}-Li($2s$) collisions. The CTMC method is based on solving the Hamiltonian equations for the motion of a three-body system (the valence electron, the Li^+ alkali-metal core, and the ionic projectile). The final quantum numbers n, ℓ, and m_ℓ were determined through a bining procedure of the classical quantities (electronic energy, electronic angular momentum, and its projection along the quantization axis), taking into account the asymptotic defects of the atomic energy levels of the Kr^{7+} ion [16] in the determination of the final $n\ell m_\ell$ distributions. The details of the bining procedure may be found in Refs. [17] and [18]. A large number of trajectories (between 7.5×10^4 and 1.25×10^5 trajectories, depending on the projectile energy) has been used to ensure statistical errors of less than 15% for the most populated $n\ell m_\ell$ sublevels ($n=7$, 8, 9, and 10). The CTMC m_ℓ distributions are reported in Tables II, III, and IV, respectively, for 7ℓ, 8ℓ, and 9ℓ sublevels. The m_ℓ distributions strongly depend on the collision energy and on the ℓ value of the sublevels.

In expression (5), in addition to the branching ratios and the cross sections, we have to choose which radiative cascade are taken into account. We have chosen to include radiative cascades up to $n=10$ levels and cascade channels for which the total branching ratio is larger than 0.010. In Table V, the number of radiative cascades taken into account is indicated for each $n\ell$ level. For each $n\ell$ level and each collision energy, we have calculated the alignment which takes into account the radiative cascades. For example, Table VI indicates the number of branches k, the upper state j, the branching ratio $\omega_k(j)$, and the alignment transfer $\xi_k(j)$ which have been used for the calculation of the $7d$ level.

Calculated polarization rates taking into account radiative cascades have been deduced from the alignment parameter for each observed transition. They are reported in Tables VII

TABLE III. CTMC m_ℓ distributions (%) versus the projectile energy (in keV amu^{-1}) for single electron capture into 8ℓ sublevels during Kr^{8+}-Li($2s$) collisions.

Sublevel \ Energy		0.1	0.2	0.5	0.8	1.0	1.4	2.0	3.0	4.0	5.0
$8s$	0	100.0	100.0	100.0	100.0	100.0	100.0	100.0	100.0	100.0	100.0
$8p$	0	31.8	27.4	28.3	27.6	28.3	27.6	31.6	28.0	30.3	32.0
	±1	34.1	36.3	35.8	36.2	35.9	36.2	34.2	36.0	34.8	34.0
$8d$	0	22.6	19.7	17.6	16.8	15.3	16.1	17.2	20.4	20.9	23.1
	±1	20.7	19.1	17.1	16.3	16.4	18.1	18.6	20.3	22.7	24.4
	±2	18.0	21.1	24.1	25.3	26.0	23.8	22.8	19.5	16.8	14.0
$8f$	0	18.5	16.5	14.8	14.4	15.1	14.6	16.1	19.7	20.0	23.7
	±1	16.7	15.4	14.4	14.3	13.8	14.8	15.2	17.1	18.2	18.3
	±2	13.6	13.7	13.3	13.1	13.7	14.0	14.2	14.5	14.7	14.1
	±3	10.4	12.6	14.8	15.4	14.9	14.0	12.5	8.6	7.1	5.7
$8g$	0	15.1	14.7	12.9	14.5	15.4	14.7	17.1	20.4	26.8	25.0
	±1	14.3	14.0	13.3	14.1	15.1	12.3	14.5	19.9	18.1	16.7
	±2	11.6	12.7	11.0	11.9	9.8	12.2	12.1	11.9	11.0	11.4
	±3	9.5	9.3	10.2	9.5	9.3	10.0	7.4	5.8	5.9	7.6
	±4	7.0	6.6	9.0	7.3	8.1	8.1	7.5	2.3	1.5	1.8
$8h$	0	11.2	12.9	12.1	14.2	12.4	16.0	21.6	21.6	19.3	17.9
	±1	11.5	9.5	11.1	12.0	12.9	15.2	15.3	16.8	15.4	16.3
	±2	10.4	10.2	9.8	9.6	9.2	10.7	9.7	9.4	11.3	12.7
	±3	9.3	9.0	9.0	8.7	8.7	6.9	6.7	7.0	8.0	8.0
	±4	6.8	7.9	8.4	7.2	7.3	5.1	5.0	4.1	4.8	3.6
	±5	6.5	6.9	5.7	5.4	5.7	4.2	2.5	1.9	0.9	0.4
$8i$	0	9.9	9.6	12.1	13.4	13.3	16.5	14.0	14.6	14.8	16.7
	±1	9.8	10.6	10.7	11.8	12.9	14.1	13.8	13.3	13.6	14.8
	±2	8.7	8.2	9.1	9.4	9.4	9.8	11.0	12.8	12.6	11.6
	±3	9.2	7.5	7.8	7.6	7.4	7.5	8.0	8.8	9.2	9.0
	±4	7.3	7.2	6.6	5.6	5.7	4.5	5.8	5.1	5.4	4.9
	±5	5.5	6.8	4.8	4.8	4.2	2.9	2.9	1.9	1.4	1.3
	±6	4.4	4.8	4.8	4.2	3.8	2.9	1.6	0.9	0.4	0.0
$8k$	0	10.1	8.7	11.0	12.5	13.7	14.7	15.1	14.0	12.9	14.5
	±1	9.7	8.5	10.8	11.2	12.4	13.6	13.2	13.4	13.6	14.1
	±2	7.3	7.7	8.2	9.3	10.1	11.2	12.7	12.3	11.9	12.0
	±3	7.3	7.0	6.8	7.4	6.8	7.1	8.1	9.9	9.6	9.3
	±4	7.6	6.0	5.8	5.1	4.9	4.5	4.3	5.4	6.3	5.5
	±5	5.5	6.6	4.4	3.6	3.8	2.5	2.0	1.6	1.7	1.7
	±6	4.5	5.5	4.1	3.9	2.8	2.1	1.2	0.3	0.3	0.2
	±7	3.1	4.4	4.4	3.3	2.4	1.7	1.0	0.2	0.1	0.0

and VIII together with the calculated polarization degrees obtained without taking into account radiative cascades. The cascade effects are found to be depolarizing for transitions from $n=9$ whereas the polarization degrees of transitions from $n=7$ and 8 sublevels are enhanced because of alignment transfer from upper levels. The radiative cascade effects are found to be weak for transitions from $n=8$ and 9, but for transitions from $n=7$ sublevels, significant deviations are found between the polarization rates calculated without radiative cascades and including radiative cascades.

On the whole, the behavior of the experimental polarization degrees with the projectile energy is fairly reproduced by the CTMC calculations including the radiative cascades. Some representative examples are shown in Figs. 1(a)–1(c). However, some calculated values are well outside the experimental errors bars. The most serious discrepancy between the calculated values and the experimental ones are for the $7f_{5/2}$-$8d_{3/2}$, np_j-nd_{j+1} $(n=7,8)$, $8d_{5/2}$-$9p_{3/2}$, and $8d_{5/2}$-$8f_{7/2}$ transitions. It is worth noting that the experimental or calculated polarization degrees are never outside the limits $P_{\min}$ and $P_{\max}$ of the polarization degrees (see Table IX). We also note that the polarization degrees approach the maximum values at large energies for transitions from the highest $n\ell$ sublevels [see Figs. 1(b) and 1(c)].

V. DISCUSSION

In our previous study of the transition polarization degrees for Ar^{8+}-Li($2s$) collisions [6,7] it was shown that the

TABLE IV. CTMC m_ℓ distributions (%) versus the projectile energy (in keV amu^{-1}) for single electron capture into 9ℓ sublevels during Kr^{8+}-Li($2s$) collisions.

Sublevel \ Energy		0.1	0.2	0.5	0.8	1.0	1.4	2.0	3.0	4.0	5.0
$9s$	0	100.0	100.0	100.0	100.0	100.0	100.0	100.0	100.0	100.0	100.0
$9p$	0	32.3	32.7	29.5	29.9	31.4	33.7	37.7	40.0	45.6	47.1
	±1	33.8	33.6	35.3	35.1	34.3	33.2	31.2	30.0	27.2	26.5
$9d$	0	23.8	22.1	20.9	21.8	22.7	24.8	28.4	31.5	35.5	37.9
	±1	20.4	19.9	19.9	20.6	20.9	22.9	23.5	25.7	25.3	25.9
	±2	17.7	19.1	19.6	18.5	17.8	14.7	12.2	8.5	6.9	5.2
$9f$	0	23.5	23.4	23.4	24.1	24.3	26.5	26.8	28.8	29.6	32.9
	±1	19.3	18.4	19.7	20.8	20.3	20.8	20.3	22.3	23.4	23.5
	±2	12.2	13.1	12.5	12.5	13.1	11.9	13.2	11.2	9.9	9.0
	±3	6.8	6.8	6.2	4.7	4.5	4.1	3.2	2.1	1.9	1.1
$9g$	0	20.7	17.3	19.2	19.3	22.2	26.1	23.5	25.8	32.8	34.4
	±1	17.4	14.9	17.6	18.0	17.6	19.1	19.1	20.4	19.8	19.4
	±2	10.9	12.5	12.0	11.3	12.5	11.4	11.9	11.5	9.7	8.6
	±3	6.7	8.4	7.3	7.9	6.4	4.6	5.5	4.5	3.9	4.7
	±4	4.7	5.5	3.5	3.2	2.3	1.8	1.9	0.7	0.2	0.2
$9h$	0	18.6	13.2	16.9	18.9	19.8	21.3	24.7	27.2	24.4	25.2
	±1	13.2	13.3	16.5	16.1	17.3	18.9	18.7	19.0	18.4	19.5
	±2	11.3	11.0	11.4	9.8	11.1	12.9	11.5	10.3	12.0	11.9
	±3	7.7	9.5	7.7	8.4	7.1	5.6	5.1	5.2	5.8	4.9
	±4	4.4	5.6	4.2	4.3	3.4	1.3	2.1	1.7	1.5	1.0
	±5	4.0	3.9	1.7	2.0	1.2	0.7	0.3	0.3	0.2	0.0
$9i$	0	16.0	16.3	18.8	21.0	19.6	21.4	18.4	19.4	19.5	22.2
	±1	13.4	14.0	16.7	15.9	18.2	17.6	17.8	17.3	18.7	20.0
	±2	9.1	10.0	10.0	10.8	10.8	12.6	13.4	13.8	13.9	12.8
	±3	8.6	5.7	6.6	6.0	5.6	5.9	6.5	6.6	5.9	4.7
	±4	4.4	5.9	4.4	3.3	3.2	2.5	2.1	2.0	1.4	1.3
	±5	3.6	3.5	1.9	2.6	1.7	0.6	0.8	0.4	0.2	0.2
	±6	2.9	2.6	1.0	0.9	0.7	0.1	0.3	0.2	0.1	0.0
$9k$	0	11.4	14.1	18.0	20.2	20.1	20.1	17.5	16.7	15.8	16.0
	±1	12.2	11.2	14.2	15.8	16.6	17.5	17.6	16.1	16.7	17.7
	±2	10.3	10.8	9.4	10.1	11.5	11.6	13.4	14.9	15.2	15.2
	±3	8.2	7.0	6.3	5.9	5.5	6.6	6.9	7.9	8.0	6.9
	±4	6.0	5.4	4.9	3.6	3.1	2.5	2.0	2.1	2.0	2.0
	±5	3.8	3.8	3.5	2.3	2.0	1.1	0.8	0.4	0.2	0.3
	±6	2.2	2.8	1.6	1.4	0.8	0.6	0.4	0.2	0.0	0.0
	±7	1.6	2.0	1.2	0.8	0.5	0.1	0.1	0.0	0.0	0.0
$9l$	0	11.6	11.1	13.7	16.5	17.5	20.7	17.3	17.4	16.5	15.2
	±1	11.0	12.0	11.8	12.5	14.8	16.5	18.3	16.7	16.2	16.3
	±2	9.3	8.5	9.8	10.2	11.0	11.4	12.6	14.3	15.1	15.0
	±3	5.0	6.4	7.5	6.7	6.0	5.3	6.6	7.7	8.1	8.6
	±4	5.4	5.9	4.7	4.7	4.3	3.0	2.2	2.0	1.9	2.0
	±5	3.9	4.7	3.7	3.7	2.4	1.6	1.0	0.3	0.2	0.3
	±6	2.7	3.2	3.0	2.1	1.7	1.1	0.6	0.0	0.0	0.0
	±7	2.7	2.0	1.9	1.3	0.7	0.5	0.2	0.0	0.0	0.0
	±8	4.3	1.7	0.8	0.4	0.3	0.2	0.0	0.0	0.0	0.0

variations of the CTMC calculated m_ℓ distributions with the projectile energy for the upper levels of the transitions reflect well those of the calculated polarization degrees. More correctly, this should be valid for the polarization degrees calculated without including the cascade effects. Therefore, as shown in Fig. 1(a), it is impossible to conclude about the m_ℓ distributions from the experimental polarization degrees and conversely about the polarization degrees from the knowledge of only the m_ℓ distributions without estimating the cascade effects. In some cases, as for the polarization

TABLE V. Number of radiative cascades taken into account in the calculation of the alignment.

Level	Number of radiative cascades
$7d$	20
$7f$	16
$7h$	8
$7i$	8
$8p$	9
$8d$	13
$8f$	7
$8g$	6
$8h$	4
$8i$	4
$8k$	4
$9p$	6
$9g$	3
$9h$	3
$9i$	3
$9k$	3
$9l$	3

degrees of transition from upper levels $n\ell$ with large values of ℓ, this may be found to be possible [see Figs. 1(b) and 1(c)]; but, even in that case it cannot be generalized, as seen, for example, for the $n=7$ level where the cascade effects are found to be quite important (see Tables VII and VIII, transitions $6g$-$7h$ and $6h$-$7i$).

In the following, we analyze in detail the variations of the polarization degrees for the Kr^{8+}-Li($2s$) collision, calculated without taking into account the cascade effects, in terms of the calculated m_ℓ distributions (Tables II, III, and IV). This is done for some upper levels of the transitions for which the polarization degrees have been reported in Tables VII and VIII. Then, from the knowledge of the electronic potential-energy curves of the $\{Kr^{7+}+Li\}^{+}$ molecular system, we tentatively draw some conclusions about the collisional mechanisms responsible for the variations of the polarization degrees.

As seen in Tables II, III, and IV, for a given $n\ell$ level, the m_ℓ distribution tends generally to be peaked on low m_ℓ values at large energies; then, with decreasing energies, it enlarges more or less and large m_ℓ values can be significantly populated. However, the $n\ell m_\ell$ distributions have quite different behaviors with the collision energy. As discussed later on in the paper, this is due to the energy-dependent efficiency of the various dynamical couplings contributing to the population of the $n\ell m_\ell$ sublevels. In particular, this competition between the dynamical couplings is probably responsible for most of the oscillations which may be seen in several $n\ell m_\ell$ distributions. However, some fluctuations in the distributions may result as well from the statistical errors in the CTMC calculated distributions ($\leqslant 15\%$ for the most populate $n\ell m_\ell$ sublevels, as indicated above). In order to illustrate, for a given $n\ell$ level, the strong correlation between the variation with energy of an m_ℓ distribution and that of the polarization degree of a corresponding transition (that is issuing from this $n\ell$ level), calculated

TABLE VI. Number of branches k, upper state j, branching ratios (ω), and alignment transfer which have been used to calculate the alignment parameter for the $7d$ level.

		Radiative cascade							
Branch k	State j	ω	state	ω	state	ω	State i	$\omega_k(j)$	$\xi_k(j)$
1	$7d$					1.000	$7d$	1.000	0.76000
2	$8p$					0.117	$7d$	0.117	0.34533
3	$9p$					0.081	$7d$	0.081	0.34533
4	$10p$					0.069	$7d$	0.069	0.34533
5	$8d$			0.167	$7f$	0.497	$7d$	0.083	0.51649
6	$8d$			0.223	$8p$	0.117	$7d$	0.026	0.25555
7	$9d$			0.078	$7f$	0.497	$7d$	0.039	0.51649
8	$9d$			0.137	$8f$	0.135	$7d$	0.018	0.51649
9	$9d$			0.161	$9p$	0.081	$7d$	0.013	0.25555
10	$10d$			0.063	$7f$	0.497	$7d$	0.031	0.51649
11	$7f$					0.497	$7d$	0.497	0.64718
12	$8f$					0.135	$7d$	0.135	0.64718
13	$8f$	0.338	$8d$	0.167	$7f$	0.497	$7d$	0.028	0.44260
14	$9f$					0.057	$7d$	0.057	0.64718
15	$10f$					0.029	$7d$	0.029	0.64718
16	$8g$			0.109	$7f$	0.497	$7d$	0.054	0.59296
17	$9g$			0.115	$7f$	0.497	$7d$	0.057	0.59296
18	$10g$			0.113	$7f$	0.497	$7d$	0.056	0.59296
19	$10g$			0.074	$8f$	0.135	$7d$	0.010	0.59296
20	$9h$	0.186	$8g$	0.109	$7f$	0.497	$7d$	0.010	0.56078

TABLE VII. Theoretical polarization rates (%) calculated from m_ℓ distributions versus the projectile energy (in keV amu^{-1}) for lines corresponding to the observed $\Delta n=0$ and $\Delta n=1$ transitions. (1) Without radiative cascade effects. (2) Including radiative cascade effects.

Energy / Transition	0.1		0.2		0.5		0.8		1.0	
	(1)	(2)	(1)	(2)	(1)	(2)	(1)	(2)	(1)	(2)
$7p_{1/2}$-$7d_{3/2}$	−5.4	5.5	−10.3	3.0	−11.5	−1.4	−7.0	−2.1	−15.6	−3.2
$7p_{3/2}$-$7d_{5/2}$	−4.3	4.4	−8.2	2.4	−9.1	−1.2	−5.6	−1.7	−12.4	−2.5
$7d_{3/2}$-$7f_{5/2}$	3.8	5.9	8.1	4.1	−12.5	−2.7	−18.2	−4.6	−17.6	−5.0
$7d_{5/2}$-$7f_{7/2}$	3.4	5.3	7.2	3.6	−11.2	−2.4	−16.1	−4.1	−15.6	−4.4
$8p_{1/2}$-$8d_{3/2}$	5.3	6.0	−2.6	1.3	−10.4	−3.8	−13.7	−5.8	−16.0	−6.8
$8p_{3/2}$-$8d_{5/2}$	4.3	4.8	−2.0	1.1	−8.3	−3.0	−10.9	−4.6	−12.7	−5.4
$8d_{5/2}$-$8f_{7/2}$	9.1	7.4	4.2	3.5	−0.3	0.3	−1.5	−0.1	−0.7	0.6
$6f_{5/2}$-$7d_{3/2}$	−1.0	1.1	−2.0	0.6	−2.2	−0.3	−1.4	−0.4	−3.0	−0.6
$6f_{7/2}$-$7d_{5/2}$	−1.5	1.6	−2.9	0.9	−3.2	−0.4	−2.0	−0.6	−4.3	−0.9
$6g$-$7h$	−7.3	11.2	−6.8	10.6	−4.9	14.7	−6.8	17.5	−1.2	19.7
$6h$-$7i$	7.3	12.8	−5.5	9.0	−4.0	13.4	3.8	18.2	8.1	21.7
$7d_{3/2}$-$8p_{1/2}$	0.0	0.0	0.0	0.0	0.0	0.0	0.0	0.0	0.0	0.0
$7d_{5/2}$-$8p_{3/2}$	−0.4	0.3	−1.3	−0.1	−1.1	−0.3	−1.3	−0.4	−1.1	−0.4
$7f_{5/2}$-$8d_{3/2}$	1.1	1.2	−0.5	0.3	−2.0	−0.8	−2.6	−1.1	−3.1	−1.3
$7f$-$8g$	11.6	11.3	12.1	11.8	6.3	9.4	10.8	13.3	10.2	13.9
$7g$-$8h$	9.1	10.2	6.8	9.0	9.1	13.4	11.8	16.2	10.8	16.5
$7h$-$8i$	10.3	12.0	8.6	10.9	11.9	15.3	14.4	18.8	16.2	20.8
$7i$-$8k$	12.2	12.5	7.5	9.5	12.5	14.6	16.2	18.8	19.9	22.4
$8d_{3/2}$-$9p_{1/2}$	0.0	0.0	0.0	0.0	0.0	0.0	0.0	0.0	0.0	0.0
$8d_{5/2}$-$9p_{3/2}$	−0.2	0.0	−0.1	0.0	−0.9	−0.2	−0.8	−0.2	−0.4	0.0
$8f$-$9g$	20.5	19.0	15.9	14.7	21.8	20.3	22.1	20.7	25.1	26.5
$8g$-$9h$	18.9	17.9	16.0	15.2	23.8	22.6	23.2	22.2	26.5	25.4
$8h$-$9i$	19.5	18.8	20.1	19.2	26.7	25.7	27.1	26.2	29.0	28.0
$8i$-$9k$	21.0	20.2	20.1	19.4	24.7	24.0	27.8	27.1	29.8	29.0
$8k$-$9l$	15.0	15.2	19.7	19.2	22.8	22.5	25.8	25.2	28.6	28.0

without taking into account the cascade effect, let us consider a few typical examples.

For the $8p$ level, the populations of the $m_\ell=\pm1$ sublevels are the largest over all the energy range, while the $m_\ell=0$ sublevel has a population approaching these at some energies. It turns out that the polarization degrees are negative and approach zero when the populations of the $m_\ell=0$ and ±1 sublevels are nearly equal. For the $9p$ level, the populations of the $m_\ell=\pm1$ sublevels are the largest up to 1 keV amu^{-1} where the population of the $m_\ell=0$ sublevel increases quickly. Consequently, the polarization degree for the $8d_{5/2}$-$9p_{3/2}$ transition is negative up to 1 keV amu^{-1}, then becomes positive and increases at high energies.

In the case of the $7d$ level, the populations of the $m_\ell=\pm2$ sublevels are the largest over all the energy range. Consequently, the polarization degrees of the $7p$-$7d$ and $6f$-$7d$ transitions are found to be negative. For the $8d$ level, the energy variations of the m_ℓ distributions are quite different. The $m_\ell=0$ sublevel is the most populated at the lowest energy (0.1 keV amu^{-1}); then its population decreases to a minimum at 1 keV amu^{-1} and increases above this energy. However, the populations of the $m_\ell=\pm2$ sublevels are the largest in the 0.2–2 keV amu^{-1} energy range and go to a maximum at 1 keV amu^{-1}. Consequently, the polarization degrees of the $8p$-$8d$ and $7f$-$8d$ transitions are positive at 0.1 keV amu^{-1}, decrease to a negative minimum at 1 keV amu^{-1}, then increase and become positive above 2 keV amu^{-1}.

Finally, let us consider the nh levels. For the $7h$ level, the $m_\ell=\pm4,\pm5$ sublevels are the most populated or have populations comparable to that of the $m_\ell=0$ sublevel up to 1.4 keV amu^{-1}. Above this energy, the population of the $m_\ell=0$ sublevel is the largest and increases continuously. The populations of $m_\ell=\pm1$, ±2, and ±3 sublevels are nearly constant up to an energy increasing with the value of m_ℓ (from 1.4 to 3 keV amu^{-1}), and then increase. As a result, the polarization degree for the $6g$-$7h$ transition is negative up to 1 keV amu^{-1} and then increases quickly. However, for the $8h$ level, the population of the $m_\ell=0$ sublevel is the largest over all the energy range, except at 0.1 keV amu^{-1}, and increases with the energy up to 3 keV amu^{-1}. The populations of the other m_ℓ sublevels decrease with m_ℓ and oscillate. Consequently, the polariza-

TABLE VIII. Theoretical polarization rates (%) calculated from m_ℓ distributions versus the projectile energy (in keV amu^{-1}) for lines corresponding to the observed $\Delta n=0$ and $\Delta n=1$ transitions. (1) Without radiative cascade effects. (2) Including radiative cascade effects.

Energy / Transition	1.4		2.0		3.0		4.0		5.0	
	(1)	(2)	(1)	(2)	(1)	(2)	(1)	(2)	(1)	(2)
$7p_{1/2}$-$7d_{3/2}$	−16.3	−2.9	−8.5	−1.0	−1.0	0.1	−6.6	2.0	−1.2	4.5
$7p_{3/2}$-$7d_{5/2}$	−12.9	−2.3	−6.8	−0.8	−8.0	0.1	−5.3	1.6	−1.0	3.6
$7d_{3/2}$-$7f_{5/2}$	−20.6	−4.2	−17.1	−2.7	−17.6	−0.6	−11.1	2.9	−6.5	5.6
$7d_{5/2}$-$7f_{7/2}$	−18.2	−3.7	−15.1	−2.4	−15.6	−0.6	−9.9	2.6	−5.8	5.0
$8p_{1/2}$-$8d_{3/2}$	−10.5	−3.6	−7.5	−1.7	1.3	4.4	7.4	8.2	13.9	12.6
$8p_{3/2}$-$8d_{5/2}$	−8.3	−2.9	−6.0	−1.4	1.1	3.5	5.9	6.6	11.2	10.2
$8d_{5/2}$-$8f_{7/2}$	1.0	2.6	4.1	5.3	12.2	11.7	15.1	14.2	18.5	17.1
$6f_{5/2}$-$7d_{3/2}$	−3.1	−0.6	−1.7	−0.2	−2.0	0.0	−1.3	0.4	−0.2	0.9
$6f_{7/2}$-$7d_{5/2}$	−4.5	−0.8	−2.4	−0.3	−2.8	0.1	−1.9	0.6	−0.3	1.3
$6g$-$7h$	0.4	23.6	7.1	25.2	16.5	27.6	19.5	29.0	18.3	29.5
$6h$-$7i$	13.2	25.8	14.6	28.5	22.2	30.2	21.9	30.2	21.0	30.4
$7d_{3/2}$-$8p_{1/2}$	0.0	0.0	0.0	0.0	0.0	0.0	0.0	0.0	0.0	0.0
$7d_{5/2}$-$8p_{3/2}$	−1.3	−0.3	−0.4	−0.1	−1.2	0.0	−0.7	0.1	−0.3	0.3
$7f_{5/2}$-$8d_{3/2}$	2.0	−0.7	−1.5	−0.3	0.3	0.9	1.5	1.7	2.9	2.6
$7f$-$8g$	8.1	14.1	12.9	18.0	26.1	26.4	28.1	27.8	25.5	26.9
$7g$-$8h$	18.3	22.4	22.6	24.9	24.7	26.8	24.7	28.0	26.5	29.3
$7h$-$8i$	20.9	25.1	22.0	26.4	24.8	28.4	26.1	29.2	27.5	29.9
$7i$-$8k$	23.7	26.5	26.5	29.4	28.6	30.9	28.1	30.8	29.0	31.1
$8d_{3/2}$-$9p_{1/2}$	0.0	0.0	0.0	0.0	0.0	0.0	0.0	0.0	0.0	0.0
$8d_{5/2}$-$9p_{3/2}$	0.1	0.2	1.0	0.5	1.5	0.7	2.7	1.1	3.1	1.2
$8f$-$9g$	28.7	26.7	27.4	25.9	31.0	29.1	33.8	31.6	33.5	31.9
$8g$-$9h$	30.7	29.5	31.3	30.1	32.1	30.7	31.6	30.5	33.0	31.9
$8h$-$9i$	31.7	30.7	31.1	30.2	31.7	30.8	32.8	32.0	34.0	33.0
$8i$-$9k$	31.7	30.9	32.1	31.4	32.4	31.8	32.7	32.1	33.1	32.4
$8k$-$9l$	31.1	30.5	32.7	32.2	33.4	33.0	33.5	33.0	33.3	32.9

tion degree of the $7g$-$8h$ transition is positive, oscillates up to 1 keV amu^{-1}, increases quickly, and finally decreases at the largest energy. For the $9h$ level, the populations of the m_ℓ sublevels are quite similar to those of the $8h$ level, but the population of the $m_\ell=0$ sublevel is comparatively larger. Then, the polarization degree for the $8g$-$9h$ transition takes large positive values over all the energy range.

Now the different variations of the m_ℓ distributions with energy for the various $n\ell$ levels may be analyzed in terms of dynamical couplings involved in the collision. In previous works for Ar^{8+} projectiles [6,7] we have shown, by a qualitative analysis of the electronic potential-energy curves of the $\{X^{7+}+\mathrm{Li}\}^{+}$ molecular system ($X\equiv O$, Ar), that radial and rotational couplings, combined with the projectile-core electron effect and the Stark effect due to the ionized target, are responsible for the final $n\ell m_\ell$ distributions. We proceed in the following to a similar discussion in the case of Kr^{8+} projectiles. The electronic energy curves for the $\{Kr^{7+}+\mathrm{Li}\}^{+}$ molecular system have been previously calculated for the Σ electronic states [1] and are shown in Fig. 2. Obvi-

TABLE IX. Minimum and maximum values $P_{\min}$ and $P_{\max}$ of the polarization rates for the observed transitions.

Transition	$P_{\min}$	$P_{\max}$
$p_{1/2}$-$d_{3/2}$	−70.4	47.9
$p_{3/2}$-$d_{5/2}$	−53.8	39.6
$d_{3/2}$-$f_{5/2}$	−84.3	44.8
$d_{5/2}$-$f_{7/2}$	−73.1	40.6
$d_{3/2}$-$p_{1/2}$	0.0	0.0
$d_{5/2}$-$p_{3/2}$	−2.5	4.9
$f_{5/2}$-$d_{3/2}$	−11.9	11.0
$f_{7/2}$-$d_{5/2}$	−17.2	15.5
f-g	−90.4	42.6
g-h	−93.5	41.0
h-i	−95.3	39.9
i-k	−96.5	39.1
k-l	−97.3	37.9

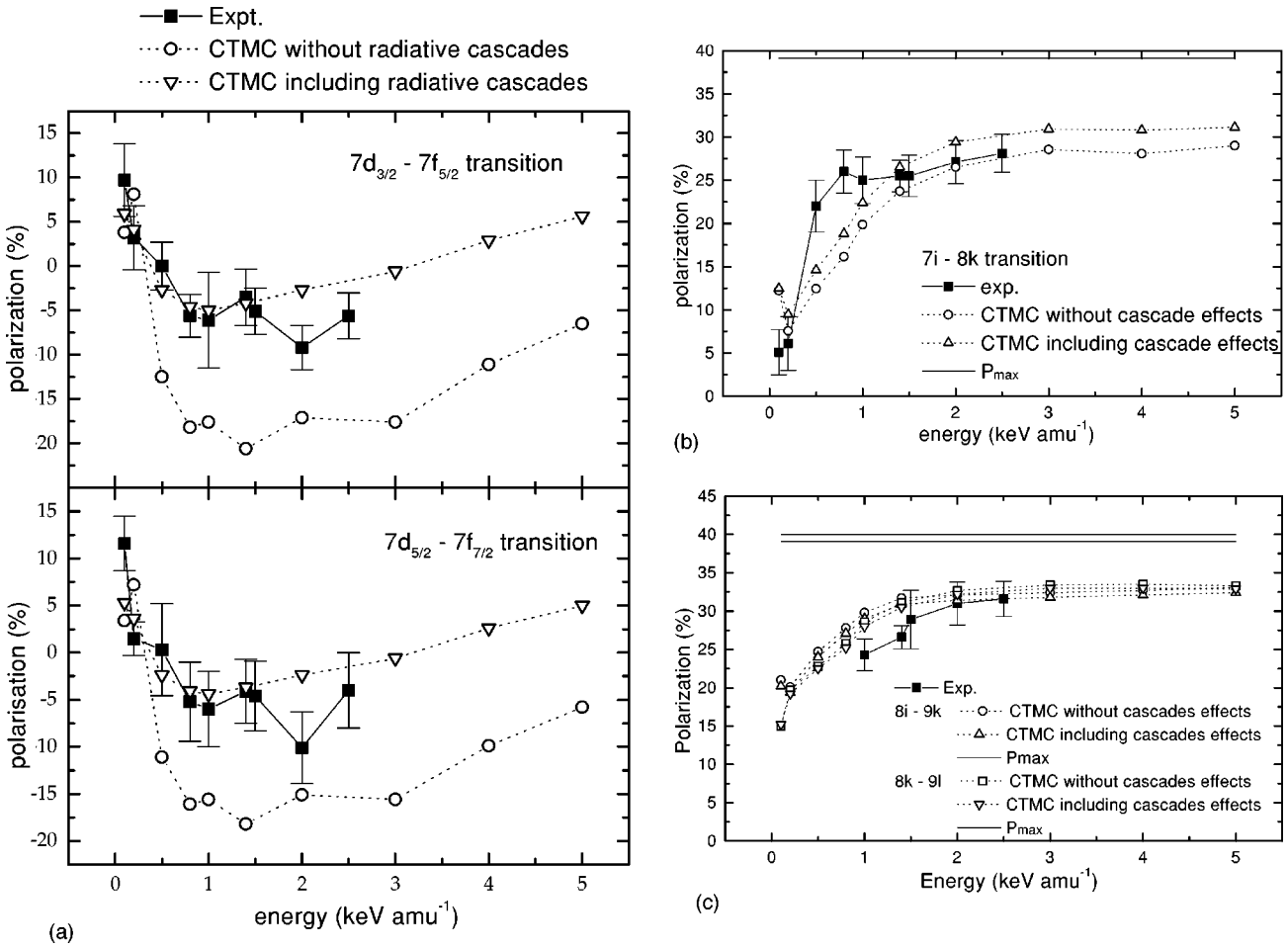

FIG. 1. Experimental and CTMC calculated polarization degrees of lines corresponding to $n\ell$-$n'\ell'$ transitions. (a) $7d_{3/2}$-$7f_{5/2}$ and $7d_{5/2}$-$7f_{7/2}$ transitions. (b) $7i$-$8k$ transition. (c) $8i$-$9k$ and $8k$-$9l$ transitions (these lines were not resolved experimentally).

ously, the Π electronic states and other electronic states of higher symmetries should also participate in the couplings. But, since the entrance channel is a Σ electronic state, it is presently sufficient to discuss the Σ electronic states. These states show up several avoided crossings with the entrance channel. In particular, they occur in the region of internuclear distance $R \cong 15-20$ a.u. for the avoided crossings associated with the $7d$, $8s$, $8p$, $7f$, and $8d$ levels of Kr^{7+}, and in the range $R \cong 22-32$ a.u. for those associated with the $9s$, $9p$, $8f$, and $9d$ levels. These avoided crossings are responsible for the primary radial couplings leading to electron capture into the $n=7$, 8, and 9 levels and of the so-called projectile core-electron effect previously discussed (see [1] for Kr^{8+} and also references therein for Ar^{8+} and O^{8+}). This core-electron effect is more efficient when the energy splitting at the avoided crossing is large, and it varies strongly with the projectile energy. At large energies the avoided crossings become adiabatic. When the energy decreases the radial couplings become first more efficient for the avoided crossings with large energy splittings. Consequently, the electron-capture cross sections go through maxima which occur at decreasing energies with decreasing energy splittings. At high energy, most of the couplings at the avoided crossings go to zero and the electron-capture

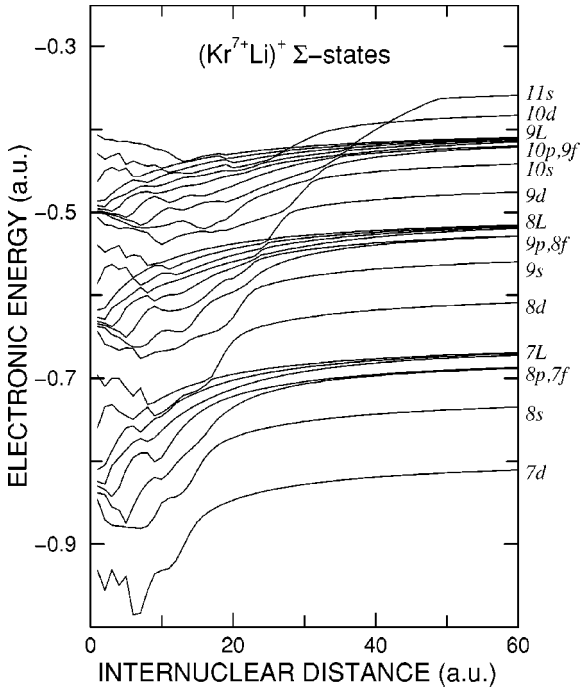

FIG. 2. Calculated electronic energies (a.u.) versus the internuclear distance (a.u.) for $\{Kr^{7+}+Li\}^+$ Σ states.

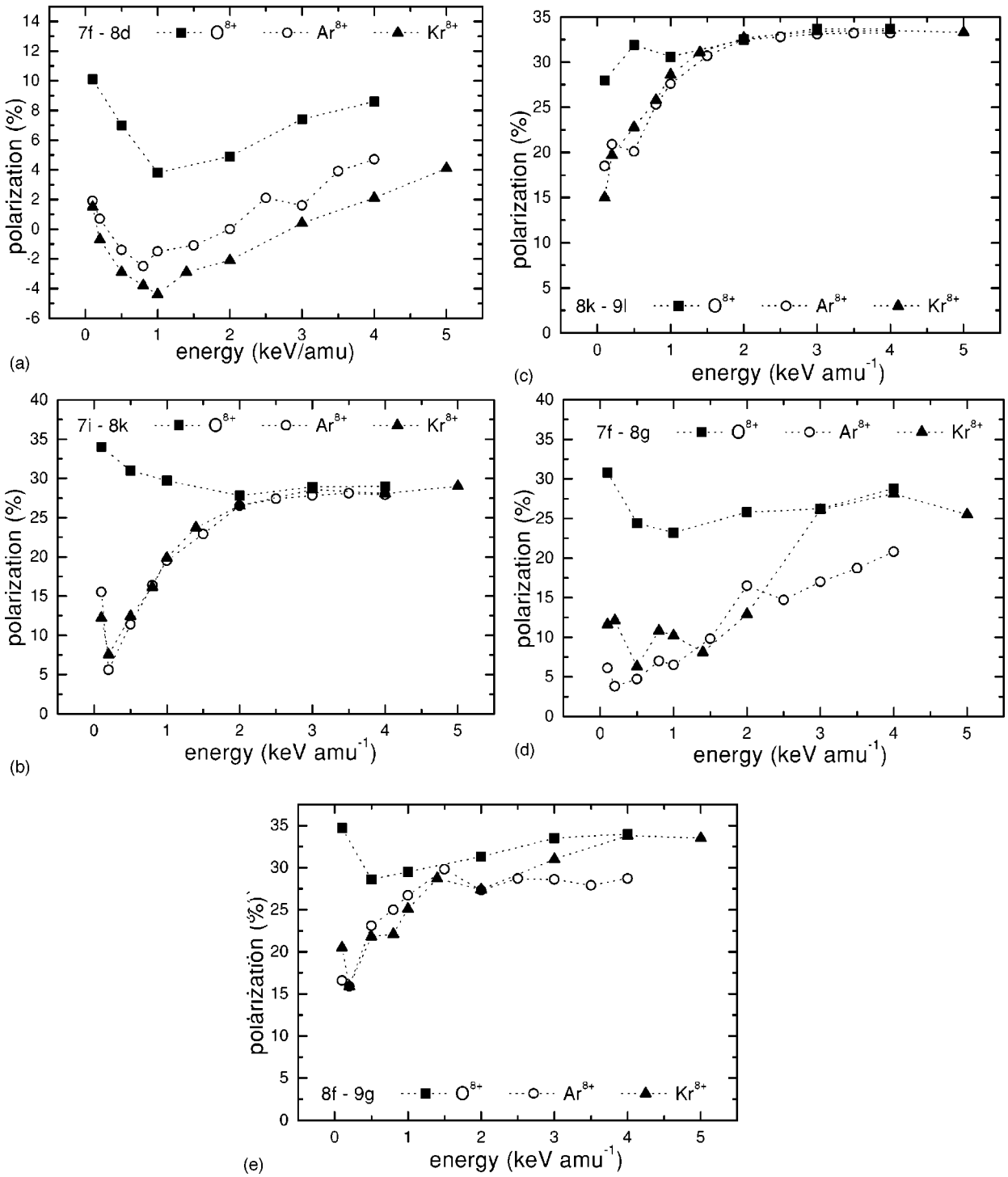

FIG. 3. CTMC calculated polarization degrees without taking into account the radiative cascades of lines corresponding to $n\ell$-$n'\ell'$ transitions. (a) $7f$-$8d$ transition. (b) $7i$-$8k$ transition. (c) $8k$-$9l$ transition. (d) $7f$-$8g$ transition. (e) $8f$-$9g$ transition.

cross section for these levels decreases. In contrast, the cross sections for electron capture into $n\ell$ states with large ℓ values should increase with energy due to the Stark effect of the residual ion. At much higher energies, rotational couplings between levels of different n may cause a decrease of these cross sections.

In the case of the $\{Kr^{7+}+Li\}^{+}$ molecular system, it may be seen that the $7d$ level has the largest energy splitting with the entrance channel. This level is then populated mainly by the primary radial coupling. That means that the $m_\ell=0$ sublevel is first populated and then the population is redistributed nearly equally to larger m_ℓ sublevels by postintrashell rotational couplings. We have about the same situation in the case of the population of the m_ℓ sublevels of the $8d$ level, where a large energy splitting is also observed with the entrance channel. For the $9d$ level, however, the energy split-

ting is much smaller. In that case, the $m_\ell = 0$ sublevel is first populated and its population is quickly redistributed. With increasing energies, because of the Stark effect and intershell rotational couplings, the $m_\ell = 0$ population increases while those of the $m_\ell = \pm 2$ sublevels decrease. In the case of Ar^{8+} projectiles, the same situation was also observed, but, for the same value of n, the effect of the projectile core electron is less important than for Kr^{8+} projectiles. This can be seen for the $7f$-$8d$ transition [Fig. 3(a)], where the polarization degrees for Ar^{8+} and Kr^{8+} have nearly the same behavior, but the polarization degrees in the case of Ar^{8+} take larger values and go through a minimum at lower energy than for Kr^{8+}. We may draw similar conclusions concerning the couplings responsible for the m_ℓ distributions of the np levels.

As for the $\{Ar^{7+} + Li\}^+$ molecular system, the manifolds of levels $n\ell$ (with $\ell \geqslant 5$) are degenerate at large internuclear distances. Therefore, the lowest values of m_ℓ should be more populated with increasing energies, by Stark coupling and intershell rotational couplings, and the more quickly the larger n. For transitions from these upper levels $n\ell$ with large values of ℓ, the polarization degrees for Kr^{8+}-Li($2s$) and Ar^{8+}-Li($2s$) collisions should vary similarly with energy. This is indeed observed in Figs. 3(b) and 3(c) for the polarization degrees of the $7i$-$8k$ and $8k$-$9l$ transitions. However, in the case of Kr^{8+}, the variations with energy of the m_ℓ distributions of the $7h$ level are quite different from what is observed for the other $n\ell$ levels with large ℓ (see Tables II, III, and IV). This seems to be associated with the core-electron effect which persists over a larger energy range for the low values of ℓ of the $n=7$ level. Concerning this, it is worth noting the parallelism of the energy curves associated with the $7h$ and $7i$ electron-capture channels, observed in the range $R \cong 8-15$ a.u.

At large internuclear distances, the ng levels are degenerate with the $n\ell$ levels ($\ell \geqslant 5$), while the nf levels are nearly degenerate with the $(n-1)p$ levels. It can be seen from Fig. 2 that the potential-energy curves associated with the nf and ng channels show smooth avoided crossings at $R \cong 16-18$ a.u. for $n=7$, $R \cong 24-27$ a.u. for $n=8$, and $R \cong 37-40$ a.u. for $n=9$. Such avoided crossings were not observed in the case of the $\{Ar^{7+} + Li\}^+$ molecular system, where both the nf and ng levels are degenerate also with the $n\ell$ levels ($\ell \geqslant 5$). Figures 3(d) and 3(e) show comparatively the polarization degrees for the $7f$-$8g$ and $8f$-$9g$ transitions for Ar^{8+} and Kr^{8+} projectiles. At low energies, the polarization degrees are higher for Kr^{8+} than for Ar^{8+} because of more efficient primary radial couplings. One should expect that at high energies, the polarization degrees increase similarly for the two projectiles, because of the Stark effect and intershell rotational couplings. However, it is interesting to note that they increase much faster for Kr^{8+} than for Ar^{8+}. We attribute this enhancement of the alignment for Kr^{8+}-Li($2s$) collisions at high energies to the large population of the nf levels by postcollisional radial coupling or rotational coupling with the $(n-1)p$ level [1], which is then redistributed to the ng levels by radial and rotational couplings, followed by the Stark effect.

As seen in Figs. 3(a)–3(e), the polarization degrees for all the transitions in the case of O^{8+}-Li($2s$) collisions are always positive and larger than for Ar^{8+} and Kr^{8+} projectiles. They decrease also with decreasing energies, but much less than for Ar^{8+} and Kr^{8+}. As discussed previously [6,7], the Stark effect and intershell rotational couplings are responsible for the population of low values of m_ℓ at high energy. As the energy decreases, the intershell rotational couplings decrease, while the intrashell rotational couplings remain efficient and cause the broadening of the m_ℓ distributions. At much lower energies, these intrashell rotational couplings decrease also and only the sublevels $m_\ell = 0, \pm 1$ will be populated by primary radial coupling and rotational coupling between the Σ and Π molecular states. Therefore, at very low energy, the polarization degrees should increase with decreasing energies, as it is observed for most of the transitions.

VI. CONCLUSION

In conclusion, we have shown by experimental studies of the Ar^{8+}-Li($2s$) and Kr^{8+}-Li($2s$) collisions over a large energy range that the polarization degrees of transition, from upper levels which are the most populated during the one-electron capture process, are compatible with most of the polarization degrees calculated from the m_ℓ distributions obtained from CTMC calculations. A discussion of these CTMC calculated m_ℓ distributions in terms of dynamical couplings responsible of the state-selective electron capture has been possible by an analysis of the electronic potential-energy curves for the $\{X^{7+} + Li\}^+$ molecular systems ($X \equiv O, Ar, Kr$).

[1] E. Jacquet, M. Chantepie, P. Boduch, C. Laulhé, D. Lecler, and J. Pascale, J. Phys. B **32**, 1151 (1999).
[2] A. Salin, J. Phys. (Paris) **45**, 671 (1984).
[3] D.M. Gauntt and D. Danzmann, Phys. Rev. A **46**, 5580 (1992).
[4] S. Schippers, P. Boduch, J. van Buchem, F.W. Bliek, and R. Hoekstra, J. Phys. B **28**, 3271 (1995).
[5] S. Schippers, R. Hoekstra, R. Morgenstern, and R.E. Olson, J. Phys. B **29**, 2819 (1996).
[6] C. Laulhé, E. Jacquet, P. Boduch, M. Chantepie, G. Cremer, N. Ghérardi, X. Husson, D. Lecler, and J. Pascale, J. Phys. B **30**, 1517 (1997).
[7] C. Laulhé, E. Jacquet, G. Cremer, J. Pascale, P. Boduch, G. Rieger, M. Chantepie, and D. Lecler, Phys. Rev. A **55**, 1088 (1997).
[8] C. Laulhé, E. Jacquet, P. Boduch, M. Chantepie, N. Ghérardi, X. Husson, D. Lecler, and J. Pascale, J. Phys. B **30**, 2899 (1997).
[9] U. Fano and J.H. Macek, Rev. Mod. Phys. **45**, 553 (1973).
[10] C.D. Lin and J.H. Macek, Phys. Rev. A **35**, 5005 (1987).
[11] M. Klapish, Comput. Phys. Commun. **2**, 239 (1971).
[12] J. Reader, N. Acquista, and V. Kaufman, J. Opt. Soc. Am. B **8**, 538 (1991).

[13] E. Jacquet, P. Boduch, M. Chantepie, M. Druetta, D. Hennecart, X. Husson, D. Lecler, F. Martin-Brunetière, R.E. Olson, J. Pascale, and M. Wilson, Phys. Scr. **49**, 154 (1994).
[14] R. Abrines and I.C. Percival, Proc. Phys. Soc. London **88**, 861 (1966).
[15] R.E. Olson and A. Salop, Phys. Rev. A **16**, 531 (1977).
[16] C.E. Theodosiou, M. Inokuti, and S.T. Manson, At. Data Nucl. Data Tables **19**, 473 (1986).
[17] E. Jacquet, J. Pascale, P. Boduch, M. Chantepie, and D. Lecler, J. Phys. B **28**, 2221 (1995).
[18] C. Laulhé, E. Jacquet, G. Cremer, J. Pascale, P. Boduch, G. Rieger, D. Lecler, M. Chantepie, and J.L. Cojan, Phys. Rev. A **52**, 3803 (1995).